Halo Structure of the Island of Inversion Nucleus ^{31}Ne

T. Nakamura,[1] N. Kobayashi,[1] Y. Kondo,[1] Y. Satou,[1] N. Aoi,[2] H. Baba,[2] S. Deguchi,[1] N. Fukuda,[2] J. Gibelin,[3] N. Inabe,[2] M. Ishihara,[2] D. Kameda,[2] Y. Kawada,[1] T. Kubo,[2] K. Kusaka,[2] A. Mengoni,[4] T. Motobayashi,[2] T. Ohnishi,[2] M. Ohtake,[2] N. A. Orr,[3] H. Otsu,[2] T. Otsuka,[5] A. Saito,[5] H. Sakurai,[2] S. Shimoura,[5] T. Sumikama,[6] H. Takeda,[2] E. Takeshita,[2] M. Takechi,[2] S. Takeuchi,[2] K. Tanaka,[2] K. N. Tanaka,[1] N. Tanaka,[1] Y. Togano,[2] Y. Utsuno,[7] K. Yoneda,[2] A. Yoshida,[2] and K. Yoshida[2]

[1]*Department of Physics, Tokyo Institute of Technology, 2-12-1 O-Okayama, Meguro, Tokyo 152-8551, Japan*
[2]*RIKEN Nishina Center, Hirosawa 2-1, Wako, Saitama 351-0198, Japan*
[3]*LPC-ENSICAEN, IN2P3-CNRS et Université de Caen, F-14050, Caen Cedex, France*
[4]*International Atomic Energy Agency (IAEA), NAPC/Nuclear Data Section, P.O. Box 100, Wagramer Strasse 5, A-1400 Vienna, Austria*
[5]*Center for Nuclear Study (CNS), University of Tokyo, RIKEN campus, Hirosawa 2-1, Wako, Saitama 351-0198, Japan*
[6]*Department of physics, Tokyo University of Science, Chiba 278-8510, Japan*
[7]*Japan Atomic Energy Agency, Tokai, Ibaraki 319-1195, Japan*
(Received 9 July 2009; published 22 December 2009)

The cross sections for single-neutron removal from the very neutron-rich nucleus ^{31}Ne on Pb and C targets have been measured at 230 MeV/nucleon using the RIBF facility at RIKEN. The deduced large Coulomb breakup cross section of 540(70) mb is indicative of a soft $E1$ excitation. Comparison with direct-breakup model calculations suggests that the valence neutron of ^{31}Ne occupies a low-ℓ orbital (most probably $2p_{3/2}$) with a small separation energy ($S_n \lesssim 0.8$ MeV), instead of being predominantly in the $1f_{7/2}$ orbital as expected from the conventional shell ordering. These findings suggest that ^{31}Ne is the heaviest halo system known.

DOI: 10.1103/PhysRevLett.103.262501 PACS numbers: 21.10.Gv, 21.60.Cs, 25.60.Gc, 27.30.+t

The neutron halo is a weakly bound exotic nuclear state where the valence neutrons are spatially decoupled from a tightly bound core and the wave function extends into the classically forbidden region. The novel quantum nature of the nuclear halo has provoked extensive experimental and theoretical studies [1–3]. In spite of this, only a handful of neutron halo systems have been experimentally identified, all of which are neutron-rich light isotopes of He through C. More generally, the halo has become recognized as a common feature of weakly bound few-body systems [2,4]. In this context it is of considerable interest to establish the existence and conditions of formation of halos in heavier neutron-rich nuclei.

The present Letter reports on the first experimental evidence for the appearance of a halo structure in ^{31}Ne. Owing to the low one-neutron separation energy $S_n = 0.29 \pm 1.64$ MeV [5], ^{31}Ne is a candidate single-neutron ($1n$) halo system [2]. The $1n$ halo is important in understanding how single-particle states play a role in halo formation. In particular, general considerations indicate that the valence neutron should occupy an orbit with low orbital angular momentum, $\ell = 0$ or 1, where the centrifugal barrier is absent or is low enough to enhance the tunneling effect [2]. Indeed, the established $1n$ halo systems, ^{11}Be and ^{19}C, are characterized by s-wave dominated valence-neutron configurations. The formation of halos in heavier systems is, however, not expected to be a general feature as the low-ℓ condition will not occur along most of the drip line [2].

The nucleus ^{31}Ne, which has 21 neutrons ($N = 21$), is also of interest as it is predicted to reside within the so-called "island of inversion", whereby the $N = 20$ shell closure vanishes as a consequence of deformation associated with strong intruder configurations [6–8]. Indeed, the neighboring nuclei such as ^{32}Na [9], ^{30}Ne [10] and, most recently, ^{32}Ne [11] are known experimentally to lie within the island [12]. In the conventional shell model the ^{31}Ne valence neutron occupies the $1f_{7/2}$ orbital and the development of an extended neutron distribution is inhibited by the high centrifugal barrier. The existence of a halo structure would thus imply a significant modification in the shell structure such as the lowering of the $2p_{3/2}$ orbital or the elevation of the $2s_{1/2}$ orbital. Note that the experimental knowledge concerning ^{31}Ne thus far has been limited to its particle stability [13] and binding energy (albeit with a poor precision) [5].

The present work is the first reaction study of ^{31}Ne and concentrates on the Coulomb breakup to probe the low-lying electric dipole ($E1$) strength. In the case of a weakly bound, spatially extended system such as a halo, a strong enhancement of the $E1$ strength (or soft $E1$ excitation) occurs close to threshold ($E_x \sim 1$ MeV). In principle, one can map the $E1$ strength distribution ($dB(E1)/dE_x$) through an exclusive measurement of the momenta of beamlike fragments in Coulomb breakup [14–18]. However, such measurements demand relatively intense beams, while the energy-and-angle integrated inclusive Coulomb breakup cross sections investigated here do not, and are sufficient to identify soft $E1$ excitations and hence possible halos. Indeed, such measurements were employed in some of the pioneering work on ^{11}Li [19].

The experiment was performed at the RI-beam factory (RIBF) operated by the RIKEN Nishina Center and the Center for Nuclear Study, University of Tokyo. The ^{31}Ne secondary beam was produced via bombardment of a thick Be target by a beam of 345 MeV/nucleon ^{48}Ca ions with an intensity of ~60 particle nA. The fragments were separated using the superconducting RI-beam separator BigRIPS [20,21]. The ^{31}Ne secondary beam was incident on lead (3.37 g/cm^2) and carbon targets (2.54 g/cm^2) at the entrance of the ZeroDegree Spectrometer (ZDS), with an intensity of ~5 particles/s. Background corrections were obtained from a run without target. The mean energy of ^{31}Ne at the center of the target was 234(230) MeV/nucleon for the Pb(C) target and the momentum spread of the ^{31}Ne beam was $\Delta P/P = \pm 3\%$. The beam particles were identified event-by-event by measuring the energy loss (ΔE), magnetic rigidity ($B\rho$) and time-of-flight (TOF) using the standard beamline detectors in the second stage of BigRIPS [11,21]. The particle-identification spectrum thus obtained is shown in Fig. 1 in terms of the atomic number (Z) and mass-to-charge ratio (A/Z), and demonstrates the clear separation of ^{31}Ne.

The ^{30}Ne fragments were collected by tuning the rigidity of the ZDS to center the momentum distribution. The particle-identification spectrum of the fragments, shown in the inset of Fig. 1, was derived from measurements of the ΔE in an ionization chamber at the final image of the ZDS, the TOF (target-final image) and the $B\rho$ using a set of PPACs at a dispersive focus of the ZDS. The inclusive one-neutron removal cross sections (σ_{-1n}) were thus derived from the number of ^{31}Ne ions counted before the target and the number of ^{30}Ne fragments registered at the final image of the ZDS. The transmission efficiency of $95 \pm 3\%$ through the ZDS, estimated using a Monte Carlo simulation and a calibration run using the secondary beam, was

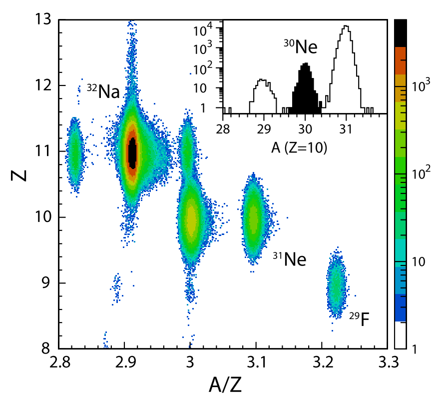

FIG. 1 (color online). Particle-identification spectrum for the secondary beam provided by BigRIPS. Inset: Particle-identification spectrum for neon isotopes in the ZDS, after selecting ^{31}Ne ions before the target.

incorporated in the extraction of σ_{-1n}. To obtain such a high transmission, the ^{31}Ne beam momentum acceptance was restricted to $\Delta P/P \leq 2\%$ in the analysis.

Measurements of σ_{-1n} were also made for a ^{19}C beam on the Pb(C) target at a mean energy of 243(238) MeV/nucleon. For the halo nucleus ^{19}C, the $E1$ strength function has already been established from an exclusive breakup measurement [15]. As such, the cross sections for ^{19}C provide a reference for the inclusive measurements.

The measured σ_{-1n} for ^{31}Ne and ^{19}C with the Pb and C targets are listed in Table I. Most significantly, the ratios of $\sigma_{-1n}(\mathrm{Pb})/\sigma_{-1n}(\mathrm{C})$ for ^{31}Ne and ^{19}C are as high as 7–9, much larger than the ratio estimated for nuclear breakup only, which is about 1.7–2.6. This demonstrates that $\sigma_{-1n}(\mathrm{Pb})$ is dominated by Coulomb breakup, as is typical for a halo nucleus [14–19].

The Coulomb breakup component of the $1n$ removal cross section on Pb, which is dominated by $E1$ excitations, $\sigma_{-1n}(E1)$, was deduced by subtracting the nuclear component estimated from $\sigma_{-1n}(\mathrm{C})$. To do this, it is assumed that $\sigma_{-1n}(\mathrm{C})$ arises entirely from the nuclear contribution, and that the nuclear component for the Pb target scales with the parameter Γ, as in,

$$\sigma_{-1n}(E1) = \sigma_{-1n}(\mathrm{Pb}) - \Gamma\sigma_{-1n}(\mathrm{C}), \tag{1}$$

where Γ was estimated to be ~1.7–2.6. The lower limit is from the ratio of target + projectile radii, as in Ref. [19], while the upper bound is derived from the Serber model [22]. The Coulomb breakup cross section was thus deduced to be $\sigma_{-1n}(E1) = 540 \pm 70$ mb for ^{31}Ne, where the uncertainty in Γ is incorporated in the error estimate. Significantly, $\sigma_{-1n}(E1)$ for ^{31}Ne is nearly as high as that for ^{19}C (Table I).

The dominance of the Coulomb breakup for the reaction on Pb and the deduced $\sigma_{-1n}(E1)$ of some 0.5 b is indicative of a soft $E1$ excitation, which is characteristic of $1n$ halo structure. The relevance of the large inclusive Coulomb breakup cross section to a soft $E1$ excitation can be understood as follows. The total inclusive Coulomb breakup cross section $\sigma(E1)$ can be expressed in terms of the integration over excitation energy E_x of the $E1$ strength distribution ($dB(E1)/dE_x$) folded with the $E1$ virtual photon number $N_{E1}(E_x)$ [23]:

TABLE I. Single-neutron removal cross sections (σ_{-1n}) for ^{31}Ne and ^{19}C on Pb and C targets at the incident energies shown. The ratio of the measured cross sections and the deduced Coulomb breakup cross sections are also listed.

Reaction	$\bar{E}/A$ (MeV)	σ_{-1n} (mb)	$\frac{\sigma_{-1n}(\mathrm{Pb})}{\sigma_{-1n}(\mathrm{C})}$	$\sigma_{-1n}(E1)$ (mb)
^{31}Ne + Pb	234	712(65)	9.0(1.1)	540(70)
^{31}Ne + C	230	79(7)		
^{19}C + Pb	243	969(34)	7.4(4)	690(70)
^{19}C + C	238	132(4)		

$$\sigma(E1) = \int_{S_n}^{\infty} \frac{16\pi^3}{9\hbar c} N_{E1}(E_x) \frac{dB(E1)}{dE_x} dE_x. \quad (2)$$

Since $N_{E1}(E_x)$ is an exponentially decreasing function of E_x, $\sigma(E1)$ becomes significant only when the $E1$ strength is concentrated at low excitation energies as for a soft $E1$ excitation [19,23]. It should be noted that since $1n$ removal channel is measured here, some yield may be lost to the $2n$ or other channels lying above the $2n$ threshold ($S_{2n} = S_n + 3.4(0.3)$ MeV [5]), a feature which enhances the sensitivity to the low-lying $E1$ strength. Soft $E1$ excitations are unique in that the $B(E1)$ spectrum peaks just above threshold and results in $\sigma_{-1n}(E1)$ as large as 0.5–1 b, while the contributions from other $E1$ excitations, such as the giant dipole resonances (GDR), are negligible [19]. The validity of this picture can be confirmed by using the known $E1$ strength function of ^{19}C [15] to compute the inclusive cross section at the current incident energy. The calculated value of $\sigma_{-1n}(E1) = 610(70)$ mb is indeed consistent with the present measurement of 690(70) mb.

We now address the single-particle structure of the ground state of ^{31}Ne. Figure 2 compares the experimentally deduced $\sigma_{-1n}(E1)$ with calculations for possible valence-neutron configurations. Owing to the large uncertainty in S_n [5], the cross sections are shown as a function of S_n.

The calculations have been made in the following manner. The $^{31}\mathrm{Ne}_{\mathrm{g.s.}}$ wave function with spin parity J^π is modeled as a linear combination of single-particle configurations: $^{30}\mathrm{Ne}(0_1^+) \otimes \phi_{nlj}$, $^{30}\mathrm{Ne}(2_1^+) \otimes \phi_{n'l'j'}, \ldots,$ where ϕ_{nlj} represents the valence neutron in the nlj orbital. The first configuration describes a valence neutron coupled to the ground state of the ^{30}Ne core. The second describes

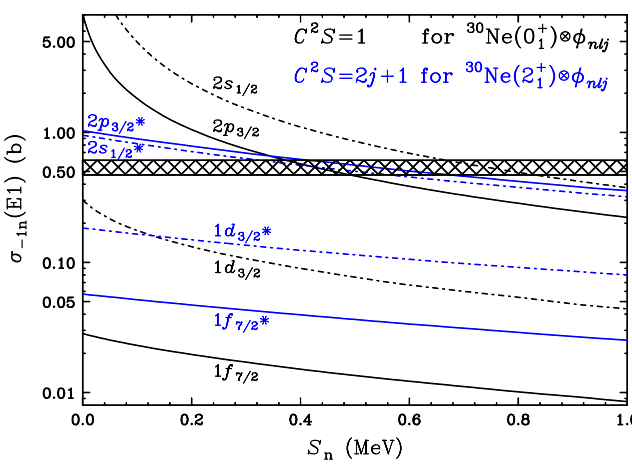

FIG. 2 (color online). The Coulomb breakup cross section for ^{31}Ne ($\sigma_{-1n}(E1) = 540(70)$ mb, hatched area) is compared with calculations for possible configurations of the valence neutron for the sum-rule limits of C^2S as a function of S_n. The solid curves are for the negative parity states, $2p_{3/2}$ and $1f_{7/2}$ coupled to $^{30}\mathrm{Ne}(0_1^+)$, while the dot-dashed curves are for the positive parity states, $2s_{1/2}$ and $1d_{3/2}$. The blue lines labeled with an asterisk are for the configurations coupled to $^{30}\mathrm{Ne}(2_1^+)$.

coupling to the first excited state of ^{30}Ne (2_1^+, $E_x = 0.801(7)$ MeV) [10,11]). Given the large effective neutron binding energies, higher-lying core states will not contribute significantly to $\sigma_{-1n}(E1)$. As such, we consider only the ^{30}Ne 0_1^+ and 2_1^+ states couple to a $2s_{1/2}$, $1d_{3/2}$, $1f_{7/2}$, and $2p_{3/2}$ valence neutron. The single-particle wave functions were derived for a Woods-Saxon potential with $r_0 = 1.24$ fm, diffuseness $a = 0.62$ fm and spin-orbit potential $V_{\mathrm{SO}} = 7.0$ MeV [24].

The $E1$ strength function is estimated based on the Coulomb direct-breakup model of a core + $1n$ system [14–16,25],

$$\frac{dB(E1)}{dE_x} \propto \sum_{(lj,J_c)} C^2S_{lj,J_c} \sum_{(l_f j_f)} |\langle \psi_{l_f j_f} | \hat{T}^{(E1)} | \phi_{nlj} \rangle|^2, \quad (3)$$

where C^2S_{lj,J_c} denotes the spectroscopic factor for $^{30}\mathrm{Ne}(J_c^\pi) \otimes \phi_{nlj}$, and the $E1$ operator $\hat{T}^{(E1)}$ involves r, the relative distance between the core and valence neutron. The wave function $\psi_{l_f j_f}$ represents the neutron scattering state in the exit channel. The core is considered to be a spectator in the reaction. As the matrix element is related to the Fourier transformation of $r\phi(r)$, the $B(E1)$ is enhanced at low E_x for a halo system [14–16].

The cross section $\sigma_{-1n}(E1)$ for each configuration is then calculated by integrating Eq. (2) up to $E_x = S_n + 3.4$ MeV(S_{2n}), assuming that above this energy decay occurs to a channel other than $1n$ emission. For C^2S, we use the maximum value of $C^2S = 1$ for a state coupled to $^{30}\mathrm{Ne}(0_1^+)$ and $C^2S = 2j + 1$ for a state coupled to $^{30}\mathrm{Ne}(2_1^+)$, which are the sum-rule limits [26]. For smaller C^2S, the cross section is reduced accordingly.

For the configurations involving $^{30}\mathrm{Ne}(0_1^+)$, the comparison in Fig. 2 shows that the data can not be reproduced by the high-ℓ configurations—$^{30}\mathrm{Ne}(0_1^+) \otimes 1d_{3/2}$ or $^{30}\mathrm{Ne}(0_1^+) \otimes 1f_{7/2}$. On the other hand, the configuration $^{30}\mathrm{Ne}(0_1^+) \otimes 2p_{3/2}$ ($J^\pi = 3/2^-$) provides an excellent agreement with the data for $S_n \sim 0.4$ MeV. Note that the agreement is good for any reasonable $C^2S(<1)$ for lower values of S_n. Similarly, the $^{30}\mathrm{Ne}(0_1^+) \otimes 2s_{1/2}$ configuration ($J^\pi = 1/2^+$) is also compatible with the data for $S_n \lesssim 0.8$ MeV.

In the case of configurations based on $^{30}\mathrm{Ne}(2_1^+)$, the cross section will be reduced as the effective neutron binding energy is increased by E_x of $^{30}\mathrm{Ne}(2_1^+)$, while the higher limit employed for C^2S will enhance it. As a result, two configurations, $^{30}\mathrm{Ne}(2_1^+) \otimes 2s_{1/2}$ with $J^\pi = (3/2, 5/2)^+$ and $^{30}\mathrm{Ne}(2_1^+) \otimes 2p_{3/2}$ with $J^\pi = (1/2 - 7/2)^-$ are compatible with the data. In short, the configurations that can explain the observed $\sigma_{-1n}(E1)$ are $^{30}\mathrm{Ne}(0_1^+) \otimes 2p_{3/2}$,$^{30}\mathrm{Ne}(0_1^+) \otimes 2s_{1/2}$, $^{30}\mathrm{Ne}(2_1^+) \otimes 2s_{1/2}$ or $\mathrm{Ne}(2_1^+) \otimes 2p_{3/2}$. These are all low-$\ell$ configurations with weak binding and, as such, are consistent with the formation of a halo.

Significantly, the naive shell model configuration of $^{30}\mathrm{Ne}(0_1^+) \otimes 1f_{7/2}$ does not contribute to the structure of

$^{31}Ne_{g.s.}$. To investigate this further, large-scale Monte Carlo shell model (MCSM) calculations employing the SDPF-M effective interaction [8] were performed. The calculations suggest that the ground state is indeed $J^{\pi} = 3/2^{-}$. This is consistent with the current findings whereby the $^{30}Ne(0_1^+) \otimes 2p_{3/2}$ configuration is favored for $^{31}Ne_{g.s.}$.

The calculated ground state is mainly composed of $3p$-$2h$, configurations as expected for an island-of-inversion nucleus. The major components of the $^{31}Ne_{g.s.}$ wave function are predicted to be $^{30}Ne(0_1^+) \otimes 2p_{3/2}(C^2S = 0.12)$, $^{30}Ne(2_1^+) \otimes 2p_{3/2}(C^2S = 0.27)$, and $^{30}Ne(2_1^+) \otimes 1f_{7/2}(C^2S = 0.25)$. This indicates that the last neutron of ^{31}Ne does indeed occupy the $p_{3/2}$ orbital with a sizable probability and will contribute strongly to the observed large soft $E1$ excitation.

The mixed ground-state configuration is consistent with ^{31}Ne lying within the island of inversion and, as such, suggests that it will be strongly deformed. It is thus interesting to describe the structure of $^{31}Ne_{g.s.}$ as a weakly bound neutron in a deformed potential [27–29]. For instance, according to the Nilsson diagram shown in Fig. 3 of Ref. [29], the 21st neutron may be located in the $[330]1/2^{-}$ or $[321]3/2^{-}$ levels which involve the $p_{3/2}$ configuration, and the $[200]1/2^{+}$ level which involves the $s_{1/2}$ configuration. It should be noted that in Refs. [27,28] the low-ℓ configurations are shown to become dominant as the separation energy tends towards zero.

In summary, we have observed a large Coulomb breakup cross section [540(70) mb] for ^{31}Ne, which is indicative of a soft $E1$ excitation. A comparison with calculations based on direct breakup suggests that $^{31}Ne_{g.s.}$ involves a valence neutron predominantly in a low-ℓ orbital with very weak binding, which is consistent with the formation of a halo. Furthermore, a dominant $f_{7/2}$ valence-neutron configuration expected from conventional shell ordering is excluded. A comparison with large-scale shell model calculations confirms that ^{31}Ne resides in the island of inversion and that it is a very loosely bound $p_{3/2}$ valence neutron that drives the soft $E1$ excitation. As such, ^{31}Ne may be the first case of a p-wave $1n$ halo. The present result could hint that, owing to changes in shell structure, halos are more abundant than expected in "heavy" neutron-rich nuclei and are intimately connected with the location of the neutron drip line. To further elucidate the structure of such weakly bound nuclei, exclusive breakup studies and precise mass and interaction cross section measurements are also needed.

We wish to extend our thanks to the accelerator staff of the RIKEN Nishina Center for their efforts in delivering the intense ^{48}Ca beam. We also appreciate the cooperation of the groups of T. Ohtsubo and H. Scheit during the ^{48}Ca beam campaign. Fruitful discussions with I. Hamamoto are greatly appreciated.

[1] I. Tanihata, Prog. Part. Nucl. Phys. **35**, 505 (1995).
[2] A. S. Jensen *et al.*, Rev. Mod. Phys. **76**, 215 (2004).
[3] B. Jonson, Phys. Rep. **389**, 1 (2004).
[4] F. Ferlaino *et al.*, Phys. Rev. Lett. **101**, 023201 (2008).
[5] B. Jurado *et al.*, Phys. Lett. B **649**, 43 (2007).
[6] E. K. Warburton, J. A. Becker, and B. A. Brown, Phys. Rev. C **41**, 1147 (1990).
[7] E. Caurier *et al.*, Phys. Rev. C **58**, 2033 (1998).
[8] Y. Utsuno *et al.*, Phys. Rev. C **60**, 054315 (1999).
[9] C. Thibault *et al.*, Phys. Rev. C **12**, 644 (1975).
[10] Y. Yanagisawa *et al.*, Phys. Lett. B **566**, 84 (2003).
[11] P. Doornenbal *et al.*, Phys. Rev. Lett. **103**, 032501 (2009).
[12] A. Gade and T. Glasmacher, Prog. Part. Nucl. Phys. **60**, 161 (2008).
[13] H. Sakurai *et al.*, Phys. Rev. C **54**, R2802 (1996).
[14] T. Nakamura *et al.*, Phys. Lett. B **331**, 296 (1994); N. Fukuda *et al.*, Phys. Rev. C **70**, 054606 (2004).
[15] T. Nakamura *et al.*, Phys. Rev. Lett. **83**, 1112 (1999).
[16] R. Palit *et al.*, Phys. Rev. C **68**, 034318 (2003).
[17] T. Aumann *et al.*, Phys. Rev. C **59**, 1252 (1999).
[18] T. Nakamura *et al.*, Phys. Rev. Lett. **96**, 252502 (2006).
[19] T. Kobayashi *et al.*, Phys. Lett. B **232**, 51 (1989).
[20] T. Kubo, Nucl. Instrum. Methods Phys. Res., Sect. B **204**, 97 (2003).
[21] T. Ohnishi *et al.*, J. Phys. Soc. Jpn. **77**, 083201 (2008).
[22] R. Serber, Phys. Rev. **72**, 1008 (1947).
[23] C. A. Bertulani and G. Baur, Phys. Rep. **163**, 299 (1988).
[24] K. Bear and P. E. Hodgson, J. Phys. G **4**, L287 (1978).
[25] A. Mengoni, T. Otsuka, and M. Ishihara, Phys. Rev. C **52**, R2334 (1995).
[26] M. H. Macfarlane and J. B. French, Rev. Mod. Phys. **32**, 567 (1960).
[27] T. Misu, W. Nazarewicz, and S. Åberg, Nucl. Phys. **A614**, 44 (1997).
[28] I. Hamamoto, Phys. Rev. C **69**, 041306(R) (2004).
[29] I. Hamamoto, Phys. Rev. C **76**, 054319 (2007).